

# Lab on a Chip

Accepted Manuscript



This is an *Accepted Manuscript*, which has been through the Royal Society of Chemistry peer review process and has been accepted for publication.

*Accepted Manuscripts* are published online shortly after acceptance, before technical editing, formatting and proof reading. Using this free service, authors can make their results available to the community, in citable form, before we publish the edited article. We will replace this *Accepted Manuscript* with the edited and formatted *Advance Article* as soon as it is available.

You can find more information about *Accepted Manuscripts* in the [Information for Authors](#).

Please note that technical editing may introduce minor changes to the text and/or graphics, which may alter content. The journal's standard [Terms & Conditions](#) and the [Ethical guidelines](#) still apply. In no event shall the Royal Society of Chemistry be held responsible for any errors or omissions in this *Accepted Manuscript* or any consequences arising from the use of any information it contains.

## ARTICLE

## Tailoring three-dimensional architectures by rolled-up nanotechnology for mimicking microvasculatures

Cite this: DOI: 10.1039/x0xx00000x

Rerngchai Arayanarakool,<sup>\*a</sup> Anne K. Meyer,<sup>a</sup> Linda Helbig,<sup>a</sup> Samuel Sanchez,<sup>b</sup> and Oliver G. Schmidt<sup>ac</sup>

Received 00th Januaray 2015,  
Accepted 00th xxxxx

DOI: 10.1039/x0xx00000x

www.rsc.org/

Artificial microvasculature, particularly as part of the blood-brain barrier, has a high benefit for pharmacological drug discovery and uptake regulation. We demonstrate the fabrication of tubular structures with patterns of holes, which are capable of mimicking microvasculatures. By using photolithography, the dimensions of the cylindrical scaffolds can be precisely tuned as well as the alignment and size of holes. Overlapping holes can be tailored to create diverse three-dimensional configurations, for example periodic nano-scaled apertures. The porous tubes which can be made from diverse materials for differential functionalization, are biocompatible and can be modified to be biodegradable in the culture medium. As a proof of concept, endothelial cells (ECs) as well as astrocytes were cultured on these scaffolds. They form monolayers along the scaffolds, are guided by the array of holes and express tight junctions. Nano-scaled filaments of cells on these scaffolds were visualized by Scanning Electron Microscopy (SEM). This work provides the basic concept mainly for an *in vitro* model of microvasculature which could also be possibly implanted *in vivo* due to its biodegradability.

### Introduction

In microvascular engineering, the scaffold for mimicking blood vessels plays an essential role in cell responses e.g. cell differentiation, cell alignment, cell elongation, gene expression, and tight-junction formation.<sup>1-9</sup> Therefore, a cylindrical structure resembling the shape of a blood vessel is a more rational approach to mimic vascular microenvironment rather than conventional rectangular ones made from microfluidic channels for *in vitro* studies.<sup>10-19</sup> As a scaffold for cell culture, the tubular structure should comprise access to nutrients. With nanotechnology methods, well-defined micro and nanostructures can be precisely fabricated to create two-dimensional (2D) architectures for exploitation in diverse fields of life science and engineering. Recently, three-dimensional (3D) architectures gained more popularity since they resemble physiological microenvironments more closely.<sup>20-24</sup> For bilayer cell culture, scaffolds should provide physical support while allowing direct contact of both cells in and outside the tube. This way, cells can create tight junctions in order to perform a biological barrier function. In general, cell-cell communication is dependent on direct physical contact or indirect contact via soluble factor regulation.<sup>21, 22, 25</sup>

Lumen formation of Endothelial cells (ECs) in 3D scaffolds of hydrogels<sup>26-30</sup> which are able to be engineered as vascular extracellular matrix<sup>31</sup> have been demonstrated as excellent systems to mimic vasculature especially for *in-vivo* applications. However, in order to mimic vasculature from arteries to capillaries, a tubular with diameters down to 10  $\mu\text{m}$  (e.g. capillary in brain) should be chosen. Hydrogels are fluids and do not offer stability or variability in size of lumen

formation, and porous cylindrical structures for cell culture have not reached diameters below 100  $\mu\text{m}$ .<sup>32</sup> Additionally, in hydrogels, vessel-like structures form spontaneously and not in a directed or designed fashion. Importantly, in hydrogel-based devices, cells embedded in 3D matrices obstruct the employment of imaging methods which are critical to nanoscale analysis. Contrarily, cells populating porous tubes can be visualized by SEM and confocal analysis with low background noise from scaffolds. Thus, the scalable, porous and tubular scaffold should provide a good platform for mimicking a microvasculature system especially for *in-vitro* applications. Such a system would have advantages for drug science due to its controllability in miniaturized dimensions (tiny holes and small tube diameter), functionalization, reproducibility, and high-resolution optical imaging.

Three-dimensional architectures fabricated by strain engineering technologies<sup>33, 34</sup> were first reported as a platform for cell culture by Mei and Huang *et al.*<sup>35, 36</sup> and established as a “*lab-in-a-tube*” application<sup>37</sup> for investigating neuronal guidance, cell mobility and cell division inside confined space.<sup>38-43</sup> In order to create uniform, continuous porous tubes for cell layer formation, we here advance our fabrication approach to roll up nanomembranes with specified arrays of holes. In our approach the diameter and number of windings can be controlled by the geometry of the thin film. Strain-engineered scaffolds with access holes and metallic patterns were reported before by Jamal *et al.*,<sup>44</sup> our work here shows scalability of tube diameter down to 10  $\mu\text{m}$  for capillaries, tunability of access holes for direct or non-direct contact of cells, tiny holes and tube curvature for homogeneous cell adhesion, and biodegradability of scaffolds. Another important aspect of our work is the use of ECs as a specific cell type

forming endothelial boundaries potentially allowing for the future use as drug-testing platforms and, gaining the possibility for evaluating speed and efficiency of drug passing through vessels (i.e. blood-brain-boundary). Though, this work mainly focus on the scaffolds as an *in vitro* model of microvasculature, the biodegradability of this three-dimensional structure is also demonstrated for the future use as an *in vivo* implant.

We demonstrate the fabrication and employment of this tubular microstructure as a cell scaffold to mimic microvasculature by culturing ECs or astrocytes around the scaffolds. ECs populate porous tubes and form a monolayer with tight junctions. Astrocytes are specifically guided to those parts of the tubes that contain holes. We fabricated metal patterns inside porous tubes offering the opportunity of specific functionalization areas or integration of a sensing system inside porous tubes. The fabrication approach of this cell scaffold was adjusted to enable the biodegradability in culture medium. This allows cells to form a mono- or bilayer where the mechanical support dissolves after layer formation. These porous tubes are capable of being integrated into microfluidic systems or rolled-up electrodes, offering the opportunity to build cylindrical-shaped microvasculature networks or to perform real-time electrical measurement on a miniaturized device.<sup>45, 46</sup>

## Materials and Methods

### Rolled-up porous tube fabrication

The porous tubes were fabricated by employing rolled-up technology and a standard photolithography as illustrated in Fig.1A. First, a glass substrate was cleaned by organic solvents (acetone and isopropanol, respectively) and dried by nitrogen before dehydration at 120°C for 5 min. A sacrificial layer was then patterned onto this substrate by using a lift-off process. This process was started by spin-coating a negative photoresist (AZ5214E, Clariant GmbH) onto this substrate (4500 rpm, 30 s) and patterned by a mask aligner (MJB4, SÜSS Microtec). Subsequently, a metallic sacrificial layer was deposited onto this substrate with patterned photoresist by using electron beam evaporation (Edwards AUTO 500 E-beam evaporator) under high vacuum ( $<10^{-4}$  Pa). Afterwards the sample was cleaned by organic solvent to remove the photoresist. Then, the second lift-off process was performed by using the same procedure as described above to create the pattern of strained nanomembrane with the array of holes by E-beam deposition prior to removing photoresist by organic solvent. In our experiment, we used copper (40 nm thick) as a sacrificial layer which can be removed by a chromium etching solution (Chromium Etch No.1, Microchem) within a few minutes. Upon the etching step, the nanomembrane with the array of holes started to roll up due to the mismatched strains of bimetallic or oxide layers forming a rolled-up porous tube.<sup>33, 34</sup> Finally, the sample was rinsed in DI water for a few minutes before drying in a critical point dryer (CPD 030, Bal-Tec AG) to avoid the structural collapse. The microtube was further coated with a 15-nm Al<sub>2</sub>O<sub>3</sub> layer by using atomic layer deposition (ALD, SavannahTM 100, Cambridge NanoTech Inc.) to strengthen the microtubes. All organic solvents were purchased from VWR GmbH.

### Characterization

The micro and nano structures of microtubes were imaged by an optical microscope (Zeiss AxioCam MR) and a SEM (Zeiss digital) with a 1-5 keV acceleration voltage. Before imaging, the samples were coated with 5-nm gold.

### Biofunctionalization of porous tube

After being fabricated by aforementioned approach, the porous tube was functionalized to promote good adhesion of cells along the scaffold. First, the tube was cleaned in oxygen plasma (30 W, 5 min) and then immersed in 1 mM 11-phosphonoundecanoic acid in toluene overnight. Afterwards, it was thoroughly rinsed in toluene, acetone, ethanol and water, respectively, and dried by nitrogen. Then it was immersed in PBS solution containing 0.1 M N-(3-dimethylaminopropyl)-N-ethylcarbodiimide (EDC) and 0.025 M N-hydroxyl sulfosuccinimide (NHS) (1 hour) followed by incubation with 0.02 mg/mL fibronectin at 37°C (1 hour). Then, the sample was immersed in EDC and NHS for one hour. In order to improve *in vitro* microvasculature, the porous tube was further coated by collagen matrices (Collagen type I, Gibco) to imitate the mechanical properties of this scaffold to soft tissue by following the protocol from manufacturer. Firstly, collagen (5 mg/mL) was mixed with sterile 10 x PBS, sterile distilled water and sterile 1 M NaOH to obtain the final collagen concentration of 3 mg/mL at pH 7. Then, the collagen solution was immediately dispensed into the microtube array and incubated at 37°C in a humidified incubator (30 min). Finally the samples were rinsed with sterile PBS before seeding cells. All chemicals were purchased from Sigma Aldrich.

### Cell Culture

The porous tubes were used as scaffolds to culture two cell lines i.e. endothelial cells (b.End3) and astrocytes (C8D1A) purchased from ATCC. Cells were cultured in cell medium (Dulbecco's Modified Eagle Medium (DMEM, Sigma Aldrich), 10 % fetal bovine serum (FBS, Sigma Aldrich), 2 mM L-Glutamine (Sigma Aldrich), 1 % Penicillin/Streptomycin (Gibco) at 37°C in a humidified atmosphere containing 5 % CO<sub>2</sub>. Cells were placed on to the micro porous tube array at a concentration of  $5 \times 10^4$  cells/mL and cultured for 2-3 weeks. The medium was refreshed every 2-3 days. Vascular endothelial growth factor, (VEGF, 10 ng/mL, PAN Biotec) was added to endothelial cells to improve vascularisation.

### Immunostaining and Fluorescent Imaging

The cell culture samples for fluorescent imaging were fixed in cold ethanol at -20°C for 10 min, then rinsed three times with PBS solution. The samples were subsequently permeabilized in 0.1 % Triton X-100/PBS (10 min) at room temperature. Afterwards, they were blocked in 1 % bovine serum albumin (BSA) in PBS for 1 hr. Then, the cell samples were incubated with primary antibody (monoclonal mouse anti-ZO-1 antibody, 10 µg/mL; Invitrogen) diluted in 1 % BSA/PBS overnight at 4°C to label ZO-1 protein. Secondary antibodies coupled to Alexa goat anti-mouse 594 (Invitrogen) were used at 1:500, phalloidin-FITC (Invitrogen) at 1:160 was used to label actin filaments, and DNA was stained using DAPI (4, 6-diamidino-2-phenylindole, Invitrogen) in PBS for 1-hour incubation at room temperature. Then, samples were rinsed in PBS three times. Finally the cell culture samples were placed between two glass cover slips prior to imaging by an inverted fluorescent microscope (AxioObserver Z1, Zeiss) or at a Zeiss LSM 780 confocal microscope.

### SEM imaging of cell culture samples

The preparation of cell culture samples for SEM imaging was done by following the protocol published before.<sup>47</sup> Briefly, the samples were incubated in 3 % glutaraldehyde (Sigma-Aldrich) in 0.1 M PBS at 37°C (15 min), then rinsed three times with PBS solution. Subsequently, they were treated in 1 % osmium tetroxide (Roth) in PBS at pH 7.4 (30 min) and then rinsed in PBS solution five times. After incubation in 1 % carbohydrazide (30 min) samples were rinsed five times in DI water (15 min). They were then incubated again in osmium tetroxide solution (30 min) before rinsing thoroughly in DI water (15 min). The samples were then dehydrated through ethanol solution series from 30 %, 50 %, 70 %, 90 % and (three times) 100 % ethanol solution over 30 min. Finally, they were dried in critical point dryer and coated with 5-nm gold.

### Biodegradation of SiO and SiO<sub>2</sub> layers

The thin films (90 nm) of SiO or SiO<sub>2</sub> which were prepared by E-beam evaporation were immersed in the culture medium and placed in an incubator at 37°C. After specific periods of time, they were thoroughly rinsed by water and dried under nitrogen flow prior to the measurement of the thickness using a profilometer. The biodegradation of this porous tube was done by culturing ECs in culture medium for 5 weeks.

### Results and discussion

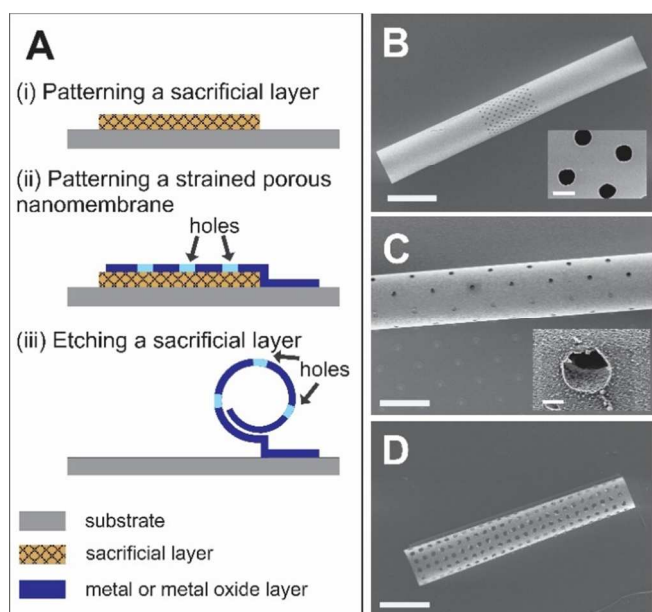


**Fig.1:** (A) Schematic of the fabrication procedure of porous tubes. (B-D) SEM image of a porous tube was fabricated by rolling up a porous strained membrane (SiO and SiO<sub>2</sub> layers). (B) The tube contains holes array in the middle with the tube diameter of 70 μm and hole diameter of 4 μm (B inset). (C) The tube (20 μm in diameter) contains holes of 2 μm (C inset). (D) The holes are rectangular-shaped with the pattern of holes along the entire tube with a tube diameter of 18 μm. The scale bars are 100 μm (B), 5 μm (B inset), 20 (C and D) and 1 μm (C inset).

### Porous tubes with diverse geometries and materials

Microtubular structures with arrays of holes can be fabricated as shown in Fig.1A. The length of porous tubes and the patterns of holes are designed and scaled down to the resolution limit of a standard photolithography. For instance, holes can be 4 μm (Fig.1B) or 2 μm (Fig.1C) in diameter. Different patterns of

holes are shown in Fig.1B (middle of a tube) and Fig.1D (entire tube) and the different shapes of holes are shown in Fig.1B (circular shape) and in Fig.1D (rectangular shape). The diameter of the tubes was tuned by altering thicknesses and deposition rates of materials to employ them as scaffolds for vascularisation at different vessel diameters (Fig.2). Physical vapour deposition allowed utilising different materials for fabrication of porous tubes (Fig.3). Importantly, one porous tube can incorporate different materials yielding diverse functionalization. For example, a gold surface inside a tube can be used for thiol functionalization and a SiO<sub>2</sub> surface outside a tube for silanization. Moreover, it is possible to make micro-metallic patterns (Fig.3J and K) allowing for spatial functionalization or real-time and vicinity sensing inside a tube.<sup>46</sup>

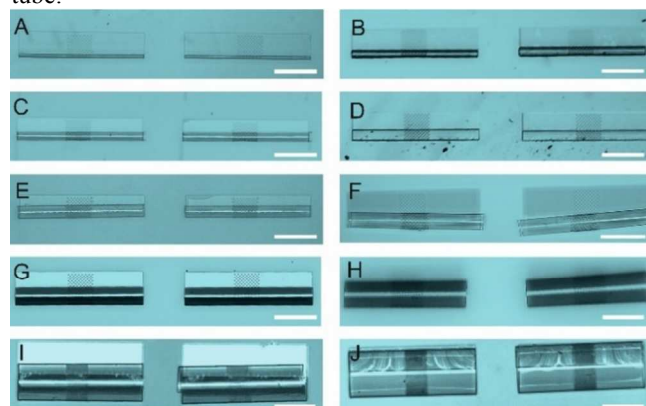


**Fig.2:** The diameters of porous tubes can be tuned by altering the thickness or the deposition rate during nanomembrane production. The tubes consist of an array of holes only in the middle part with the hole diameter of 2-4 μm and the length of the array is around 120 μm. Porous tubes were made from SiO/SiO<sub>2</sub> membranes (A-F and J), SiO<sub>2</sub>/TiO<sub>2</sub> membrane (G, H) and TiO<sub>2</sub> membrane (I). The tube diameters were approximately 15 μm (A), 30 μm (B), 40 μm (C), 50 μm (D), 60 μm (E), 70 μm (F), 80 μm (G), 125 μm (H), 170 μm (I) and 225 μm (J). Scale bars for all images are 200 μm.

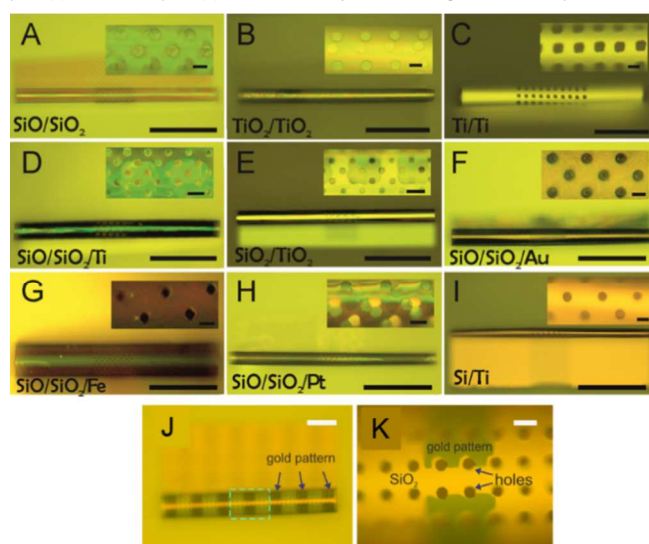


**Fig.3:** Porous tubes can be made from different materials providing versatile functionality. The tubes were made from SiO/SiO<sub>2</sub> (A), TiO<sub>2</sub>/TiO<sub>2</sub> (B), Ti/Ti (C), SiO/SiO<sub>2</sub>/Ti (D), SiO/TiO<sub>2</sub> (E), SiO/SiO<sub>2</sub>/Au (F), SiO/SiO<sub>2</sub>/Fe (G), SiO/SiO<sub>2</sub>/Pt (H), and Si/Ti (I). (J) Porous tubes with integrated gold pattern. (K) Magnified imaged of the middle of a SiO<sub>2</sub> tube with hole diameter of 4 μm and gold patterns.

Gold patterns can be used for localized functionalization such as sensing inside a tubular structure. The scale bars for all images are 200  $\mu\text{m}$ , except for (C): 15  $\mu\text{m}$ , (J): 100  $\mu\text{m}$ , and (K): 10  $\mu\text{m}$ . The insets are the magnified images of the hole array in the middle area of each porous tube. The scale bar for all insets is 5  $\mu\text{m}$  except for (C inset): 2  $\mu\text{m}$ .

After rolling up, a short membrane created a porous tube with a few ( $< 2$ ) windings (Fig. 4A) providing pass-through holes. Such tubes were suitable for exploring direct physical contact between cells inside and outside a tube. On the other hand, long membranes created a porous tube with several ( $> 2$ ) windings so that the holes in each layer did not overlap with those of neighbouring layers (Fig. 4B and 4C) could be useful for investigations of indirect communication between cells. In this case, cells cannot establish direct cell-to-cell contact because the apertures are too small for cell filament to pass. This way, communication between cells on in and outside of tube can only rely on indirect soluble factor communication.<sup>21</sup> The dimension of holes was downscaled with our fabrication approach to 2  $\mu\text{m}$  which is the limit of a standard photolithography. Overlapping holes create diverse periodic 3D configurations, for example, miniaturized apertures around the overlapping holes resulted in periodic *star-shaped* patterns (Fig. 4E and 4H) and *I-shaped* patterns (Fig. 4F and 4I). These 3D architectures were dependent on the patterns of holes, the dimensions of nanomembranes before rolling, and the diameter of the tubes which were all controllable in our approach

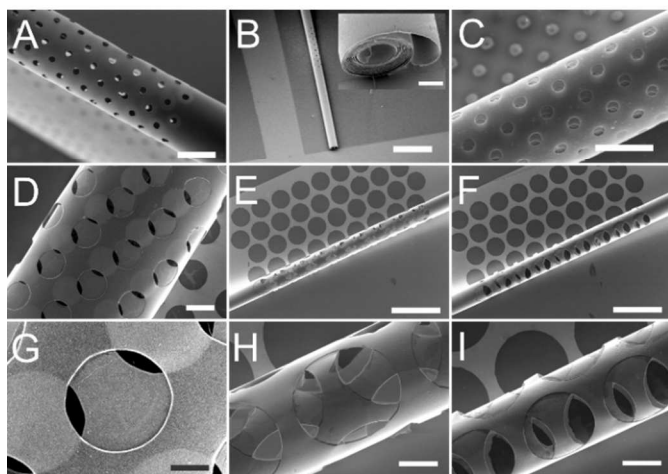


**Fig. 4:** Diverse configurations of the 3D architectures formed by rolling up a nanomembrane with holes patterns. (A) A porous tube with one winding is fabricated from a short porous membrane providing tiny pass-through holes (B) The porous tube with several windings (Fig. 4B inset) is fabricated from the long membrane without pass-through holes (C) allowing only tiny objects or molecules to pass through. (D) Nano-scaled periodic holes patterns can be made from the overlapped holes of this structure. The dimension of the original holes pattern is 4  $\mu\text{m}$  and after rolling up, the overlapped holes create smaller aperture with the dimension of 0.5  $\mu\text{m}$  by 2  $\mu\text{m}$ . The scale bar is 20  $\mu\text{m}$  (A), 100  $\mu\text{m}$  (B), 5  $\mu\text{m}$  (B inset), 10  $\mu\text{m}$  (C), 5  $\mu\text{m}$  (D), 2  $\mu\text{m}$  (D inset), 50  $\mu\text{m}$  (E and F), and 10  $\mu\text{m}$  (E inset and F inset).

#### Cell culture around porous tubes

After culturing cells around the porous tubes, we studied the cell morphology and cellular components by immunostaining. In the culture system of astrocytes on porous tubes, astrocytes grew around tubes and migrated into tubes particularly to the

patterns of holes (Fig. 5). A single confocal image at the bottom of a tube (Fig. 5A) demonstrated that cells migrated into tubes and rather adhered to the part of the tube where holes presents. In this area, in tubes with  $< 2$  windings, cells can directly contact cells outside of the tube through holes allowing direct contact communication. A single confocal image in the middle plane of a tube showed that astrocytes were also able to climb the walls of the tubes (Fig. 5B), leading to a layer of astrocytes around the circumference of the tube. In scanning electron microscopy images, filaments were visible that spread along the tubes as well as sprouting from the inside to the outside of tubes with  $< 2$  windings that allow direct passing through holes (Fig. 5C and 5D). This emphasized that the connectivity of cells inside and outside of porous tubes is changing with the amount of windings. Few windings allow direct contact and communication between cells while many windings prevent cell filaments to reach from one side to the other, this way allowing only indirect communication between cells while many windings prevent cell filaments to reach from one side to the other, this way allowing only indirect communication via soluble factors.

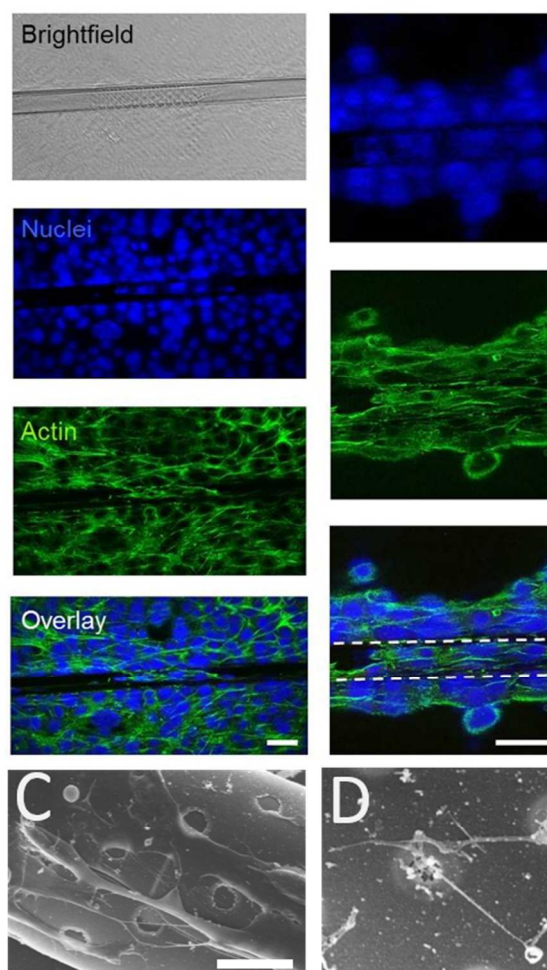
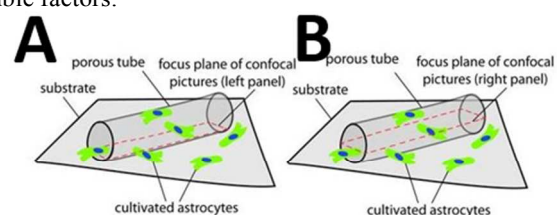


**Fig.5:** Confocal images of astrocytes around a porous tube. (A): Confocal Image taken at the bottom of sample (z-position of image slice illustrated above). (B): Confocal Image in the middle of sample (in z-direction as illustrated above). (C) SEM images of astrocytes seeded around the porous tube. (D) High-resolution of SEM allowed visualization of nano-scaled cellular components around porous tubes. The scale bar is 50  $\mu\text{m}$  (A), 10  $\mu\text{m}$  (C) and 2  $\mu\text{m}$  (D).

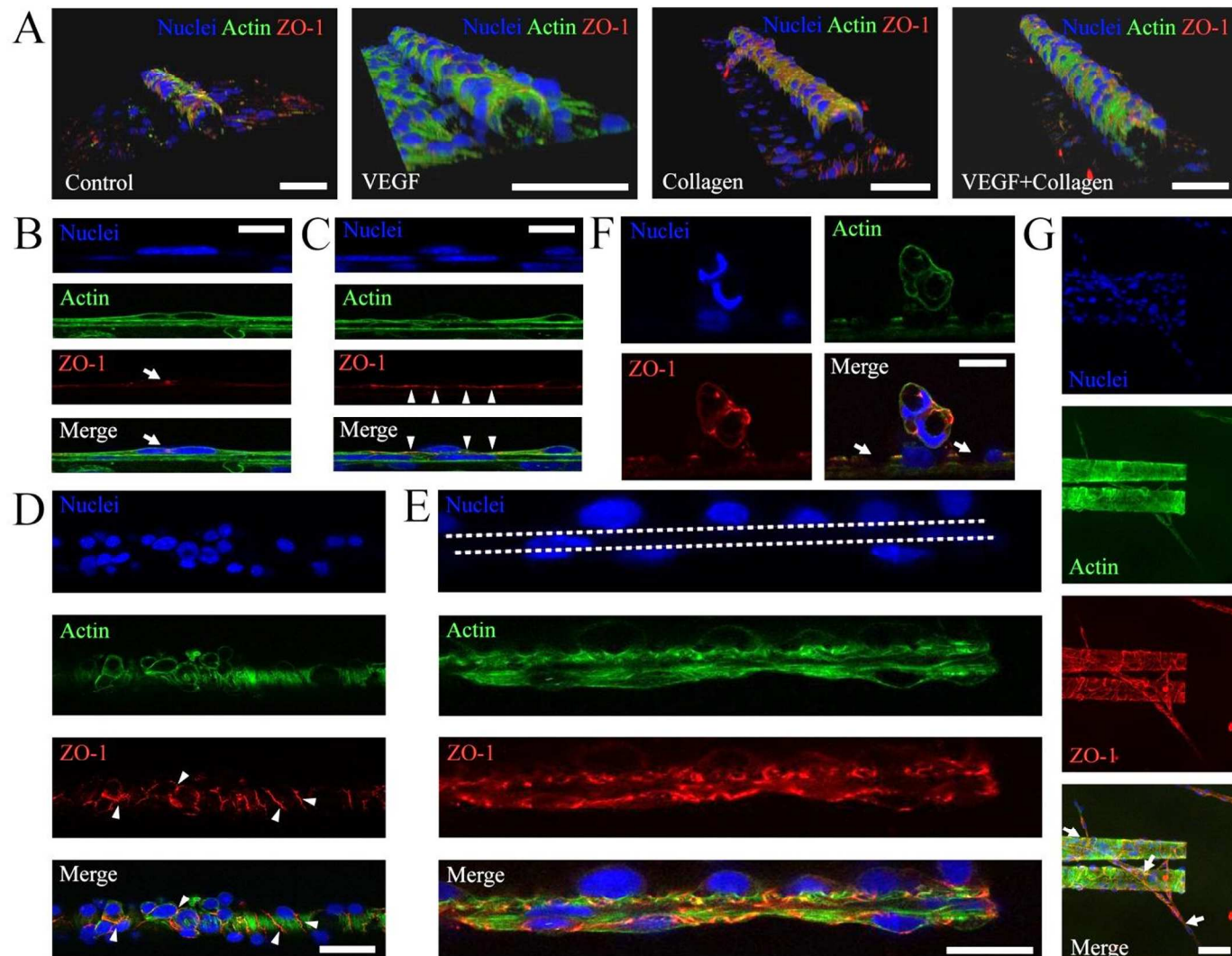


**Fig.6:** Confocal images of endothelial cells seeded on porous tubes. A) 3D Reconstructions from confocal stacks. The scale bar is 50  $\mu\text{m}$ . B, C) Tight junctions between cells (arrows, B) and between cells and porous tube (arrowheads, C). Scale bars equal 10  $\mu\text{m}$ . D) Tight junctions between cells (arrowheads) on top of tube. Scale bar equals 20  $\mu\text{m}$ . E) Endothelial bilayer formation on two sides (in and out) of the lateral tube wall. Scale bar equals 10  $\mu\text{m}$ . F) Lumen formation attaching to holes of tube (arrows). Scale bar equals 10  $\mu\text{m}$ . G) Multiple lumina form on double tubes and connect them to flat surface. Scale bar equals 50  $\mu\text{m}$ .

Recently, researchers have promoted the growth and adhesion of ECs and lumen formation by replicating the substrate stiffness of soft tissue and/or adding vascular endothelial growth factor (VEGF).<sup>48, 49</sup> Therefore, we further investigated the influence of coating with extracellular matrices such as collagen and adding VEGF (Fig.6). 3D Reconstruction of confocal stacks revealed ECs occupying the outer walls of porous tubes (Fig.6A) with or without addition of VEGF and/or collagen to the samples. When VEGF was added, more cells climbed the walls of tubes and formed tighter monolayers, as shown by the expression of ZO-1 at the cell membranes (Fig.6B and 6C). ZO-1 is a protein forming highly specialized epithelial junctions in endothelial cells. These tight junctions form a diffusion barrier to control the transport of molecules

through the cell monolayer which is a hallmark of an endothelial cell layer. Importantly, tight junctions were not only formed in between cells (Fig.6B) but also between cells and porous tubes (Fig.6C). When VEGF and collagen were added to the samples, on top of the porous tubes the cells formed a tight monolayer, as shown by tight junctions between all cells in that z-plane (Fig.6D). Across the lateral walls of the porous tubes, ECs were able to form an endothelial bilayer. This means that one layer of cells formed on the inside of the wall and the other layer on the outside of the same wall, creating a bilayer on two sides of an integrated nanomembrane (Fig.6E). When collagen was used to enhance the elasticity of the sample more lumen formation was observed. These lumina frequently spanned from the flat surface toward patterns of holes on

porous tubes (Fig.6F). The combination of VEGF and collagen on porous tube substrates was most successful in inducing vascularization from porous tubes (Fig.6G).

By using porous tubes, monolayer formation of ECs became possible for different diameters (Fig.7). This allowed mimicking of different sizes of vasculature from arteries to capillaries. In summary, porous tubes supported the production of endothelial monolayers that are capable of performing a biological barrier function, as well as bilayers and lumen formation of ECs.

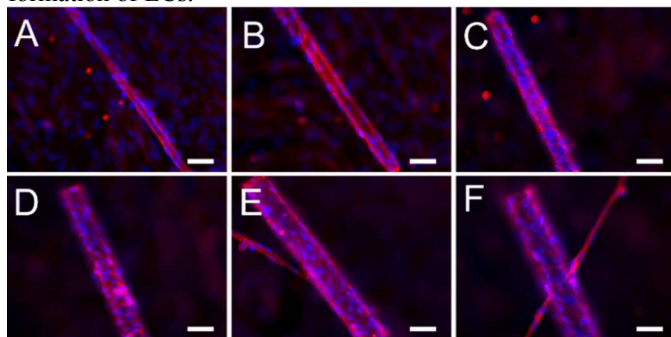


**Fig.7.** The formation of ECs monolayer at different diameters, i.e., 12  $\mu\text{m}$  (A), 20  $\mu\text{m}$  (B), 30  $\mu\text{m}$  (C), 40  $\mu\text{m}$  (D), 50  $\mu\text{m}$  (E), and 60  $\mu\text{m}$  (F). The blue channel is nucleus and the red channel is ZO-1. The scale bars for all images are 50  $\mu\text{m}$ .

### Biodegradation of porous tubes

It was reported before that thin layer of silicon oxides (SiO and SiO<sub>2</sub>) dissolve in the buffer solution.<sup>50</sup> In our regular experiments the porous tubes were made of SiO and SiO<sub>2</sub> and later coated with Al<sub>2</sub>O<sub>3</sub> using atomic layer deposition to stabilise the SiO/SiO<sub>2</sub> scaffold. Tubes coated with alumina were stable for more than 6 weeks in culture medium since alumina prevented dissolution of silicon oxides.<sup>51</sup> However, in absence of alumina, silicon oxide layers dissolved in cell culture medium. The thin-layer of these oxide membranes dissolved in the medium at a rate of around 10 nm/day (Fig.8A). We also investigated the biodegradability of porous tubes in contact with ECs culture. The rolled-up porous tubes which were made of SiO and SiO<sub>2</sub> (40 and 175 nm in thickness, respectively) and functionalized with collagen (without alumina coating) were used as scaffolds to culture ECs. The tube consisted of 4 windings of SiO/SiO<sub>2</sub> layers with the total wall thickness of around 860 nm. Cells formed a monolayer around the tube and became confluent in 2-3 weeks. They formed lumina from several positions, both on the flat substrate and around the tube as indicated by numbers 1, 2 and 3 in Fig.8B-D. The tubes which were covered by ECs started bending from the middle part after 24 days of culture (Fig.8B, C) and eventually deformed their shape after 33 days (Fig.8D). The bending of tubes was owing to the contraction force from the lumina which were connecting a tube to flat area of the sample as indicated by numbers 1, 2 and 3 in Fig.8B-D. The dissolution of thin films and deformation of porous tubes confirmed the biodegradation of these materials in culture medium. In summary, we have shown a versatile approach to fabricate tunable porous tubes for biological layer formation of ECs which can be biodegradable, functionalized and integrated into lab-in-a-tube devices for drug discovery.

### Discussion

Our versatile fabrication approach can reproducibly generate high-throughput porous tubular structures with scalable sizes of pores and tube diameters to mimic microvasculature as the size of the pores is defined by photolithography and the tube diameter is dependent on the thicknesses and deposition rates of the nanomembrane materials as depicted in Fig.2 – 4. These structures offer cylindrical shape, apertures around the tube, and the possibility of micropatterning inside porous tubes. Guidance of astrocytes and lumen formation of ECs demonstrated the proof-of-principle for the application as artificial microvasculature. Additionally, porous tubes with varied numbers of windings and diverse sizes of holes can be used for investigations of different cell-cell communication pathways. We here used tubular structures with holes to study the formation of biological barriers that require physical contact of cells. However, porous tubes can also be fabricated with several windings without pass-through holes for the investigation of indirect communication of cells. There, porous tubes act as a barrier to inhibit direct cell contact while small molecules can pass through space between windings and non-overlapping holes. It was reported that ECs directly contacting to astrocytes via 3- $\mu\text{m}$  holes exhibited heterogeneous behaviours compared to those cells which were indirectly contacted via sub-micron holes,<sup>25</sup> emphasizing the significant role of barrier for cell-cell communication. This will be the specific design criteria to make the cylindrically-shaped tubular scaffold suitable for investigation of cell responses in the ECs/Astrocytes co-culture system. Apart from this, the diameter of the tubular structure should be large enough for cells migrating inside. In addition, biodegradability enables porous tubes to stabilize lumen formation of desirable dimensions and to dissolve after formation is complete.

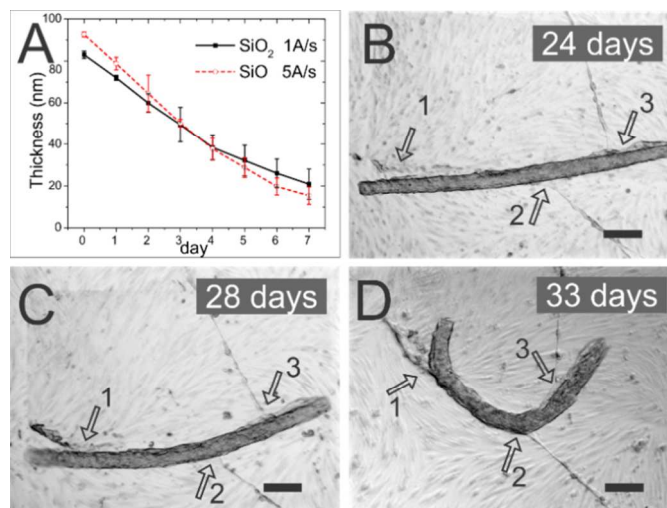


**Fig.8:** (A) The dissolution of SiO layer (dash line) and SiO<sub>2</sub> layer (solid line) in culture medium. SiO and SiO<sub>2</sub> were deposited by using E-beam evaporation with the rate of 5  $\text{\AA}/\text{s}$  and 1  $\text{\AA}/\text{s}$ , respectively. The dissolution rate in culture medium (pH 7.4) is around 10 nm/day for both layers. (B-D) The collagen-coated porous tube which was seeded by ECs was deformed in culture medium for a few weeks. ECs formed lumens on the flat surface and around the tube as indicated by numbers 1, 2 and 3. At 24<sup>th</sup> day, the porous tube started to bend from the middle. At 33<sup>rd</sup> day, the tube deformed their shape in several positions. The scale bars are 100  $\mu\text{m}$ .

### Outlook

Different functionalizations or real-time and vicinity sensing inside a tube<sup>46</sup> can be made inside our tubular structure which is difficult to perform in polymer-based devices.<sup>27, 52-54</sup> For example, one can measure nitric oxide released from ECs intrinsically to link biological functions of blood vessels i.e. vascular muscle relaxation,<sup>55-57</sup> or monitor simultaneously the confluence and development of tight junctions of ECs by measuring transendothelial electrical resistance (TEER).<sup>20</sup> In this work, we use copper as a sacrificial layer requiring the etching solution of perchloric acid and ammonium cerium nitrate which is hazardous for cells. However, in the future, one can try to use PBS solution to etch copper<sup>58</sup> or change to water-soluble polymers.<sup>59</sup> This would allow to roll up seeded cells together with the nanomembrane in PBS or water solution. Moreover, fabrication of microtubes on a substrate surface provides the opportunity to employ this structure for the field of *body on a chip* which was recently established.<sup>60-63</sup> This compartmented system will be useful as co-culture system of microvasculature of ECs and other biological systems outside the tube, for instance, mimicking the blood-brain barrier (ECs and astrocytes), or replicating the microvasculature in muscles or other organs. Therefore, rolled-up porous tubes are a next-generation structure useful as cell scaffolds for biological barrier formation and for lab-in-a-tube application.

### Acknowledgement

We thank the BIOTEC/CRTD Light Imaging Facility for excellent support with confocal microscopy. The research has received funding from the European Research Council under the European Union's Seventh Framework Programme (FP7/2007-2013)/ERC Grant Agreement 311529 and the Volkswagen foundation (no. 86 362).

### Notes

<sup>a</sup> Institute for Integrative Nanosciences, Leibniz Institute for Solid State and Materials Research Dresden, Helmholtzstraße 20, 01069, Dresden, Germany

<sup>b</sup> Max Planck Institute for Intelligent Systems, Heisenbergstr.3, D-70569, Stuttgart, Germany

<sup>c</sup> Materials Systems for Nanoelectronics, TU Chemnitz, 09107, Chemnitz, Germany

### References

1. T. Kadohama, N. Akasaka, K. Nishimura, Y. Hoshino, T. Sasajima and B. E. Sumpio, *Endothelium-Journal of Endothelial Cell Research*, 2006, 13, 43-50.
2. G. M. Riha, P. H. Lin, A. B. Lumsden, Q. Z. Yao and C. Y. Chen, *Annals of Biomedical Engineering*, 2005, 33, 772-779.
3. R. M. Nerem, R. W. Alexander, D. C. Chappell, R. M. Medford, S. E. Varner and W. R. Taylor, *American Journal of the Medical Sciences*, 1998, 316, 169-175.
4. A. B. Fisher, S. Chien, A. I. Barakat and R. M. Nerem, *American Journal of Physiology-Lung Cellular and Molecular Physiology*, 2001, 281, L529-L533.
5. L. Cucullo, M. Hossain, V. Puvanna, N. Marchi and D. Janigro, *Bmc Neuroscience*, 2011, 12.
6. O. C. Colgan, G. Ferguson, N. T. Collins, R. P. Murphy, G. Meade, P. A. Cahill and P. M. Cummins, *American Journal of Physiology-Heart and Circulatory Physiology*, 2007, 292, H3190-H3197.
7. E. Warabi, Y. Wada, H. Kajiwara, M. Kobayashi, N. Koshihara, T. Hisada, M. Shibata, J. Ando, M. Tsuchiya, T. Kodama and N. Noguchi, *Free Radical Biology and Medicine*, 2004, 37, 682-694.
8. J. M. Tarbell, *Cardiovascular Research*, 2010, 87, 320-330.
9. W. M. Weaver, S. Dharmaraja, V. Milisavljevic and D. Di Carlo, *Lab Chip*, 2011, 11, 883-889.
10. R. Booth and H. Kim, *Lab Chip*, 2012, 12, 1784-1792.
11. J. T. Borenstein, M. M. Tupper, P. J. Mack, E. J. Weinberg, A. S. Khalil, J. Hsiao and G. Garcia-Cardena, *Biomedical Microdevices*, 2010, 12, 71-79.
12. N. J. Douville, Y. C. Tung, R. Li, J. D. Wang, M. E. H. El-Sayed and S. Takayama, *Analytical Chemistry*, 2010, 82, 2505-2511.
13. Z. C. Huang, X. Li, M. Martins-Green and Y. X. Liu, *Biomedical Microdevices*, 2012, 14, 873-883.
14. S. Kruss, L. Erpenbeck, M. P. Schon and J. P. Spatz, *Lab Chip*, 2012, 12, 3285-3289.
15. S. H. Ma, L. A. Lepak, R. J. Hussain, W. Shain and M. L. Shuler, *Lab Chip*, 2005, 5, 74-85.
16. B. Prabhakarandian, M. C. Shen, J. B. Nichols, I. R. Mills, M. Sidoryk-Wegrzynowicz, M. Aschner and K. Pant, *Lab Chip*, 2013, 13, 1093-1101.
17. S. Srigunapalan, C. Lam, A. R. Wheeler and C. A. Simmons, *Biomicrofluidics*, 2011, 5.
18. P. A. Vogel, S. T. Halpin, R. S. Martin and D. M. Spence, *Analytical Chemistry*, 2011, 83, 4296-4301.
19. J. H. Yeon, D. Na, K. Choi, S. W. Ryu, C. Choi and J. K. Park, *Biomedical Microdevices*, 2012, 14, 1141-1148.
20. E. Cukierman, R. Pankov and K. M. Yamada, *Current Opinion in Cell Biology*, 2002, 14, 633-639.
21. Y. Ling, J. Rubin, Y. Deng, C. Huang, U. Demirci, J. M. Karp and A. Khademhosseini, *Lab Chip*, 2007, 7, 756-762.
22. H. Zhang, S. Dai, J. X. Bi and K. K. Liu, *Interface Focus*, 2011, 1, 792-803.
23. K. E. Sung, X. J. Su, E. Berthier, C. Pehlke, A. Friedl and D. J. Beebe, *Plos One*, 2013, 8.
24. P. Zorlutuna, N. Annabi, G. Camci-Unal, M. Nikkhah, J. M. Cha, J. W. Nichol, A. Manbachi, H. J. Bae, S. C. Chen and A. Khademhosseini, *Adv Mater*, 2012, 24, 1782-1804.
25. Y. Hayashi, M. Nomura, S. I. Yamagishi, S. I. Harada, J. Yamashita and H. Yamamoto, *Glia*, 1997, 19, 13-26.
26. L. L. Bischel, E. W. K. Young, B. R. Mader and D. J. Beebe, *Biomaterials*, 2013, 34, 1471-1477.
27. M. De Ville, P. Coquet, P. Brunet and R. Boukherroub, *Microfluidics and Nanofluidics*, 2012, 12, 953-961.
28. M. Jamal, S. S. Kadam, R. Xiao, R. Jivan, T. M. Onn, R. Fernandes, T. D. Nguyen and D. H. Gracias, *Advanced Healthcare Materials*, 2013, 2, 1142-1150.
29. S. Kim, H. Lee, M. Chung and N. L. Jeon, *Lab Chip*, 2013, 13, 1489-1500.
30. I. K. Zervantonakis, S. K. Hughes-Alford, J. L. Charest, J. S. Condeelis, F. B. Gertler and R. D. Kamm, *Proceedings of the National Academy of Sciences of the United States of America*, 2012, 109, 13515-13520.
31. H. Geckil, F. Xu, X. H. Zhang, S. Moon and U. Demirci, *Nanomedicine-Uk*, 2010, 5, 469-484.
32. B. Yuan, Y. Jin, Y. Sun, D. Wang, J. S. Sun, Z. Wang, W. Zhang and X. Y. Jiang, *Adv Mater*, 2012, 24, 890-+.
33. V. Y. Prinz, V. A. Seleznev, A. K. Gutakovskiy, A. V. Chehovskiy, V. V. Preobrazhenskii, M. A. Putyato and T. A. Gavrilova, *Physica E*, 2000, 6, 828-831.
34. O. G. Schmidt and K. Eberl, *Nature*, 2001, 410, 168-168.

35. Y. F. Mei, G. S. Huang, A. A. Solovev, E. B. Urena, I. Moench, F. Ding, T. Reindl, R. K. Y. Fu, P. K. Chu and O. G. Schmidt, *Adv Mater*, 2008, 20, 4085-+.
36. G. S. Huang, Y. F. Mei, D. J. Thurmer, E. Coric and O. G. Schmidt, *Lab Chip*, 2009, 9, 263-268.
37. E. J. Smith, W. Xi, D. Makarov, I. Monch, S. Harazim, V. A. B. Quinones, C. K. Schmidt, Y. F. Mei, S. Sanchez and O. G. Schmidt, *Lab Chip*, 2012, 12, 1917-1931.
38. S. Schulze, G. S. Huang, M. Krause, D. Aubyn, V. A. B. Quinones, C. K. Schmidt, Y. F. Mei and O. G. Schmidt, *Advanced Engineering Materials*, 2010, 12, B558-B564.
39. W. Xi, C. K. Schmidt, S. Sanchez, D. H. Gracias, R. E. Carazo-Salas, S. P. Jackson and O. G. Schmidt, *Nano Lett*, 2014, 14, 4197-4204.
40. C. S. Bausch, A. Koitmaa, E. Stava, D. Diedrich, A. Price, P. J. Resto, D. Sonnenberg, C. Heyn, W. Justin, E. Dent and R. H. Blick, *Biophys J*, 2013, 104, 329a-329a.
41. P. Froeter, Y. Huang, O. V. Cangellaris, W. Huang, E. W. Dent, M. U. Gillette, J. C. Williams and X. L. Li, *Acs Nano*, 2014, 8, 11108-11117.
42. M. R. Yu, Y. Huang, J. Ballweg, H. Shin, M. H. Huang, D. E. Savage, M. G. Lagally, E. W. Dent, R. H. Blick and J. C. Williams, *Acs Nano*, 2011, 5, 2447-2457.
43. B. Koch, S. Sanchez, C. K. Schmidt, A. Swiersy, S. P. Jackson and O. G. Schmidt, *Advanced Healthcare Materials*, 2014, 3, 1753-1758.
44. M. Jamal, N. Bassik, J. H. Cho, C. L. Randall and D. H. Gracias, *Biomaterials*, 2010, 31, 1683-1690.
45. S. M. Harazim, V. A. B. Quinones, S. Kiravittaya, S. Sanchez and O. G. Schmidt, *Lab Chip*, 2012, 12, 2649-2655.
46. C. S. Martinez-Cisneros, S. Sanchez, W. Xi and O. G. Schmidt, *Nano Lett*, 2014, 14, 2219-2224.
47. C. Heckman, S. Kanagasundaram, M. Cayer and J. Paige, 2007.
48. A. Alajati, A. M. Laib, H. Weber, A. M. Boos, A. Bartol, K. Ikenberg, T. Korff, H. Zentgraf, C. Obodozie, R. Graeser, S. Christian, G. Finkenzeller, G. B. Stark, M. Heroult and H. G. Augustin, *Nature Methods*, 2008, 5, 439-445.
49. S. Brouillet, P. Hoffmann, M. Benharouga, A. Salomon, J. P. Schaal, J. J. Feige and N. Alfaidy, *Molecular Biology of the Cell*, 2010, 21, 2832-2843.
50. S. K. Kang, S. W. Hwang, H. Y. Cheng, S. Yu, B. H. Kim, J. H. Kim, Y. G. Huang and J. A. Rogers, *Advanced Functional Materials*, 2014, 24, 4427-4434.
51. T. Chappex and K. L. Scrivener, *Cement and Concrete Research*, 2012, 42, 1645-1649.
52. E. Kang, S. J. Shin, K. H. Lee and S. H. Lee, *Lab Chip*, 2010, 10, 1856-1861.
53. L. M. Li, X. Y. Wang, L. S. Hu, R. S. Chen, Y. Huang, S. J. Chen, W. H. Huang, K. F. Huo and P. K. Chu, *Lab Chip*, 2012, 12, 4249-4256.
54. S. Zakharchenko, N. Puretskiy, G. Stoychev, C. Waurisch, S. G. Hickey, A. Eychmuller, J. U. Sommer and L. Ionov, *Journal of Materials Chemistry B*, 2013, 1, 1786-1793.
55. A. R. Butler and D. L. H. Williams, *Chemical Society Reviews*, 1993, 22, 233-241.
56. J. P. Cooke and V. J. Dzau, *Annual Review of Medicine*, 1997, 48, 489-509.
57. J. M. Mclenachan, J. Vita, R. D. Fish, C. B. Treasure, D. A. Cox, P. Ganz and A. P. Selwyn, *Circulation*, 1990, 82, 1169-1173.
58. K. Malachowski, M. Jamal, Q. R. Jin, B. Polat, C. J. Morris and D. H. Gracias, *Nano Lett*, 2014, 14, 4164-4170.
59. V. Linder, B. D. Gates, D. Ryan, B. A. Parviz and G. M. Whitesides, *Small*, 2005, 1, 730-736.
60. M. B. Esch, G. J. Mahler, T. Stokor and M. L. Shuler, *Lab Chip*, 2014, 14, 3081-3092.
61. J. B. Lee and J. H. Sung, *Biotechnology Journal*, 2013, 8, 1258-1266.
62. M. L. Shuler and M. Esch, *Journal of Tissue Engineering and Regenerative Medicine*, 2012, 6, 347-347.
63. A. Williamson, S. Singh, U. Fernekorn and A. Schober, *Lab Chip*, 2013, 13, 3471-3480.